Transactions on Additive Manufacturing Meets Medicine
Trans. AMMM, 2024, Vol. 6, No 1, Article ID 1785, 4 Pages

Infinite Science Publishing

Original Research Article

Creation and analysis of additive-manufactured CT-equivalent phantom tissue surrogates

M. Wegner[1,2*], M. Rosendal[2], N. Hinrichsen[1], D. Krause[1], and E. Gargioni[2]

[1] *Institute of Product Development and Mechanical Engineering Design, Hamburg University of Technology, Germany*
[2] *Department of Radiotherapy and Radiation Oncology, University Medical Center Hamburg-Eppendorf, Germany*
[*] *Corresponding author, email: marie.wegner@tuhh.de*

Abstract: Fused Deposition Modeling (FDM) can produce durable and cost-effective anatomical phantoms that meet specific X-ray contrast requirements. This study investigates the impact of infill patterns and densities on computed tomography (CT) numbers. Sixteen samples were created using various filaments, infill patterns, and densities. Infill densities ranged from 30% to 90% for cubic infill and from 80% to 100% for line infill. The samples were scanned with a clinical CT scanner and average Hounsfield Units (HU) and standard deviations were measured using regions of interest (ROI) on transversal CT images. The findings indicate that small variations in infill can significantly alter HU values, suggesting extensive applications for different phantom tissue types in X-ray imaging. Cubic infill is particularly suitable for lower HU values, such as those representing lung tissue, whereas line infill at different densities can produce HU values suitable for soft tissue applications, from adipose to liver.

I. Introduction

Additive manufacturing (AM) has gained significant interest for producing phantoms, particularly for X-ray applications in imaging and radiotherapy [1-3]. Phantoms are models designed to replicate geometric or anatomic properties of the human body, together with well-defined tissue properties, and are typically used for quality assurance and calibration. For example, phantoms might be used in computed tomography (CT) to replicate the X-ray attenuation properties of human tissue [2]. AM has expanded the user base for phantom manufacturing, since it offers several advantages over traditional methods, including greater geometric flexibility, reduced production time, and lower costs.

Furthermore, AM is a versatile technique that can be used directly or indirectly (e.g., for the fabrication of a mold or a sacrifice material) in phantom manufacturing. [3,4]. In particular, Fused Deposition Modeling (FDM), which is low-cost and commonly available in many commercial printers, has been successfully used for direct manufacturing in the past [2,3,5]. Through this technique, an object is produced layer by layer from a melted filament. By varying infill parameters and infill density of the printed object, it is possible to mimic different imaging properties of biological tissue [6-9]. Hong et al., for example, evaluated different infill ratios of ABS, TPU, and PLA [6]. Their study demonstrates that a wide range of CT numbers can be achieved by controlling the internal filling of these 3D printing materials, which are suitable for manufacturing lung phantoms. Another possibility for adjusting the CT numbers in AM is the use of different printing patterns, as shown by Madamesila et al. for HIPS [8], who showed that different infill patterns can affect both the CT number and the measuring uncertainty.

In the view of manufacturing anthropomorphic phantoms for CT-based studies, the purpose of this work was to analyze the CT numbers of several FDM materials by varying both infill pattern and density.

II. Material and methods

The electron density phantom CIRS Model 062 M (CIRS Tissue Simulation & Phantom Technology, Norfolk, VA, USA) was used as a standardized test environment with known properties. This phantom has various inter-changeable material inserts with well-known elemental composition, as well as electron density, like lung inhale, lung exhale, adipose, breast, muscle and liver tissue. For testing 3D printed materials and comparing their properties to those of the CIRS inserts, we designed a truncated cone in Autodesk Inventor (Autodesk, Inc., San Rafael, CA, United States) to fit into the phantom. The cone model was

exported as an STL file and printing preparation was done in Cura (Ultimaker B.V., Geldermalsen, The Netherlands), with a layer height of 0.15 mm and a line width of 0.4 mm. Finally, the model was 3D printed with the FDM printer Ultimaker S5 (Ultimaker B.V., Geldermalsen, The Netherlands) with a 2.85mm filament thickness using different filaments and infill patterns as well as varying infill densities.

We selected PLA (Das Filament, Germany), ecoPLA tough (niceshops GmbH, Austria), PLActive (Copper 3D, Chile) and PVA (PolyDissolve™ S1, Polymaker, USA) as the materials (see Fig. 1), which were printed with a cubic or line infill pattern. For a cubic infill pattern, we manufactured PLA with varied infill densities in 20% increments, ranging from 90% to 30%. For line infill, all materials were manufactured with an infill density of 90% as well as full material samples with 100% infill. PLA was also printed in a finer scale with 92%, 87%, 85%, and 80% infill, respectively. An example for infill patterns and densities in Cura can be seen in Fig. 2.

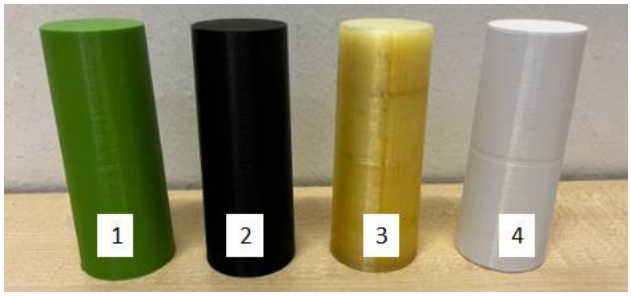

Figure 1: AM samples made from different filaments. From left to right: 1 PLAactive, 2 PLA tough, 3 PVA and 4 PLA.

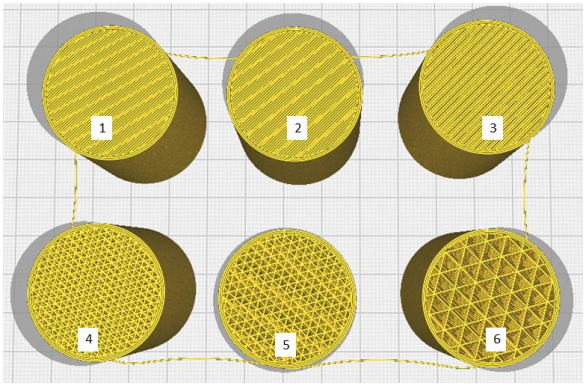

Figure 2: AM samples in Cura with different infill patterns and densities. 1 lines infill 100%, 2 lines infill 90%, 3 lines infill 80%, 4 cubic infill 90%, 5 cubic infill 50% and 6 cubic infill 30% .

The AM samples were placed inside the CIRS phantom, as shown in Fig. 3, and investigated with a Siemens SOMATOM go.Open Pro CT scanner (Siemens Healthcare GmbH, Erlangen, GER). We scanned the phantom at 100 kV with a head and a thorax protocol, filter type FLAT, and an X-ray current of 102 mA. We measured the CT numbers (in Hounsfield Units, HU) using a circular region of interest (ROI) of 25 mm in diameter in ImageJ [10] and determined mean values and standard deviation across multiple slices (slice thickness: 2 mm).

Figure 3: Set-up of the AM truncated cones placed inside the calibration phantom together with the changeable material inserts.

III. Results and discussion

Example images of the CT-scans are depicted in Fig. 4. We observed that the cubic infill patterns are visible in the CT images, resulting in non-homogeneous representation, as shown in Fig. 4. Additionally, a thicker line can be seen on the exterior of the cylinders, since each cylinder features a fully dense printed border for structural integrity (see also Fig. 2).

PLA Samples with cubic infill have HU values ranging from about -212 to about -684 HU (see Table 1) and are therefore in the range of lung tissue (around -500 HU), comparable to those of the CIRS lung materials (also listed in Table 1). For mimicking X-ray attenuation properties of soft tissues, the line infill pattern seems more appropriate, as shown in Table 2, depending on the material. A comparison between PLA and PLA though for 100% and 90% infill and the line pattern shows that the HU values are very similar (difference around 10 HU), while PLActive and PVA produce higher HU values.

As already observed in literature, it can be seen that adjusting the infill density can effectively modulate the range of HU values. In particular, a finer modulation of the infill density for PLA between 80% and 100% demonstrates that the relationship between HU and infill density is linear (see Fig. 6) [6-8]. When comparing with the CIRS materials for soft tissue (see Table 2), we observe that the tested materials can cover the whole range of CT numbers, when the appropriate relationship between infill density and CT numbers is established. Nevertheless, variations can occur in additive manufactured materials due to changes in the filament batches, therefore these measurements should be repeated when using different batches to establish the degree of reproducibility.

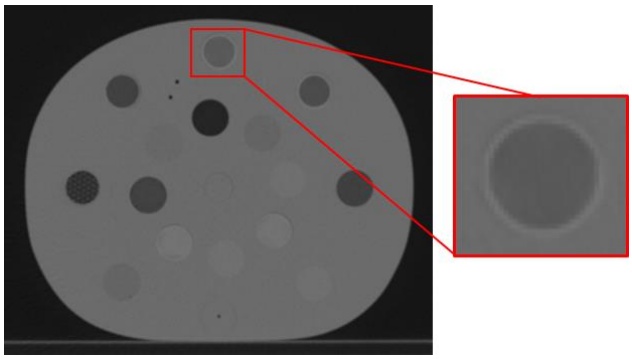

Figure 4: Transversal CT-scan of the phantom and AM samples. Sample PLA 90% line infill depicted in zoom.

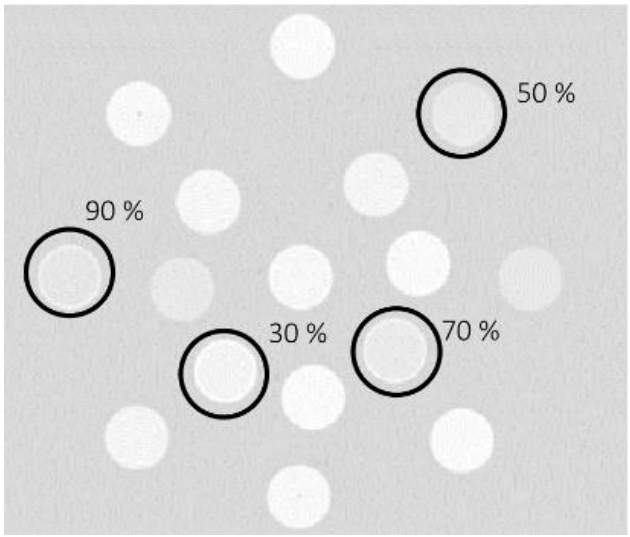

Figure 5: Transversal CT-scan with cubic infill samples highlighted.

Table 1: Overview of measured CT-numbers with standard deviations for PLA cylinders with different cubic infill densities, inserted in the CIRS phantom, obtained using the thorax scan mode of the CT scanner. The values of the CIRS materials for lung tissue, measured during the same experiment, are also listed for comparison.

Material	Infill density (%)	Mean HU-value and standard deviation
PLA	90	-212 ±64
PLA	70	-372 ±68
PLA	50	-485 ±82
PLA	30	-684 ±174
Lung inhale	-	-839 ± 13
Lung exhale	-	-497 ± 26

Table 2: Overview of measured CT-numbers with standard deviations for PLA, PLA tough, PLActive, and PVA with different line infill densities, obtained using the head and thorax scan mode of the CT scanner. The values of the CIRS materials for adipose, muscle, breast, and liver tissues,, measured during the same experiment, are also listed for comparison.

Material	Infill density (%)	Mean HU-value, standard deviation, scan protocol
PLA	100	98 ±14 Head 79 ±24 Thorax
PLA	92	95 ±10 Head
PLA	90	37 ±12 Head 31 ±15 Thorax
PLA	87	34 ±15 Head
PLA	85	15 ±13 Head
PLA	80	-40 ±11 Head
ecoPLA tough	100	95 ±14 Head 72 ±23 Thorax
ecoPLA tough	90	25 ±16 Head 20 ±23 Thorax
PLActive	100	147 ±7 Head 132 ±18 Thorax
PLActive	90	87 ±10 Head 70 ±8 Thorax
PVA	100	114 ±4 Thorax
PVA	90	66 ±14 Thorax
Adipose	-	-87 ± 14 Thorax
Breast	-	-34 ± 13 Thorax
Muscle	-	53 ± 12 Thorax
Liver	-	64 ± 12 Thorax

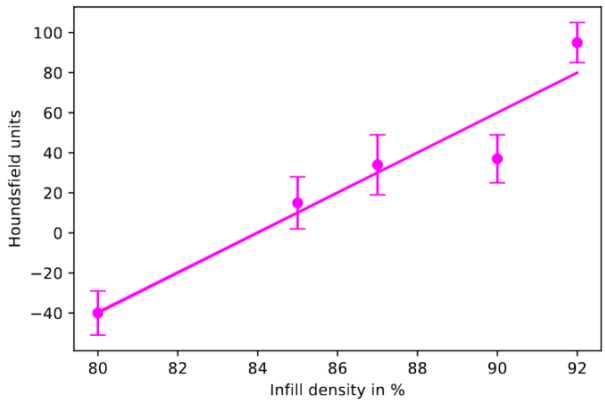

Figure 6: HU values for PLA for different line infill densities, ranging from 80% to 92%.

IV. Conclusions

We manufactured and analyzed a selection of different FDM samples with varying infill densities in CT imaging to produce tissue equivalent CT-Phantom surrogates. The results show that different HU-values can be produced using even little infill variations, which offers a broad application opportunity for different phantom tissue types in X-ray imaging. Cubic infill could be primarily interesting for lower HU values, like lung tissue, while line infill with different densities can produce HU values raging in the soft tissue applications, from adipose to liver. Overall, we observed a linear relationship between HU and infill density for PLA, which is expected to be valid also for other materials, as observed in other studies. Thus, FDM printing even with one material offers the possibility to produce a phantom with different tissue types.

In a next step the analyzed tissue surrogates will be selected for a head phantom, for which the representation of different tissues, like brain, liquor, lips, or eyes, can be made possible by choosing different infill densities for given HU values, according to the established linear relationship.

Acknowledgments

The authors state no funding involved.

Author's statement

Conflict of interest: Authors state no conflict of interest. Animal models: Indicate here under which approval you have carried out animal experiments. Informed consent: Informed consent has been obtained from all individuals included in this study.

Ethical approval: The research related to human use complies with all the relevant national regulations, institutional policies and was performed in accordance with the tenets of the Helsinki Declaration, and has been approved by the authors' institutional review board or equivalent committee.

References

[1] G. Sands, C. H. Clark, and C. K. McGarry, A review of 3D printing utilisation in radiotherapy in the United Kingdom and Republic of Ireland, Physica Medica, 115, 2023, 103143.
[2] N. Okkalidis, 3D printing methods for radiological anthropomorphic phantoms, Phys. Med. Biol. 67, 2022, 15TR04
[3] V. Filippou, C. Tsoumpas, Recent advances on the development of phantoms using 3D printing for imaging with CT, MRI, PET, SPECT, and ultrasound, Med. Phys. 45(9), 2018, pp. e740-e760.
[4] M. Wegner, E. Gargioni, D. Krause, Indirectly additive manufactured deformable bladder model for a pelvic radiotherapy phantom, Transactions on Additive Manufacturing Meets Medicine, vol. 3 (1), 2021.
[5] M. Wegner, J. Spallek, D. Krause, E. Gargioni, Comparing Technologies of Additive Manufacturing for the Development of Modular Dosimetry Phantoms in Radiation Therapy, Transactions on Additive Manufacturing Meets Medicine, vol. 2 (1), 2020.
[6] D. Hong, S. Lee, G. B. Kim, S. M. Lee, N. Kim, and J. B. Seo, Development of a CT imaging phantom of anthromorphic lung using fused deposition modeling 3D printing, Medicine, vol. 99 (1), 2020, e18617.
[7] S.Y. Kim, J.W. Park, J. Park, J.W. Jea, S.A. Oh, Fabrication of 3D printed head phantom using plaster mixed with polylactic acid powder for patient-specific QA in intensity-modulated radiotherapy, Sci. Reports 12, 2022, p. 17500.
[8] J. Madamesila, P. McGeachy, J.E. Villareal Barajas, R. Khan, Characterizing 3D printing in the fabrication of variable density phantoms for quality assurance of radiotherapy, Physica Medica, 32, 2016, pp. 242-247.
[9] S. Hatamikia, G. Kronreif, A. Unger et al., 3D printed patient-specific thorax phantom with realistic heterogenous bone radiopacity using filament printer technology, Z. Med. Phys. 32, 2022, pp. 438-452.
[10] C. A. Schneider, W. S. Rasband, K. W. Eliceiri, NIH Image to ImageJ: 25 years of image analysis. Nature Methods, vol. 9 (7), 2012, pp. 671–675.